



Nanoscale

**Whispering Gallery Mode Emission from Dye-Doped Polymer  
Fiber Cross-sections Fabricated by Near-Field  
Electrospinning**

Journal:	<i>Nanoscale</i>
Manuscript ID	NR-ART-01-2020-000147.R1
Article Type:	Paper
Date Submitted by the Author:	30-Mar-2020
Complete List of Authors:	Cheaney, Joseph; University of California Riverside Hsieh, Stephen; University of California Riverside, Material Science and Engineering Myung, Nosang; University of California-Riverside, Department of Chemical and Environmental Engineering Haberer, Elaine; University of California, Riverside, Department of Electrical and Computer Engineering

SCHOLARONE™  
Manuscripts

# 1 **Whispering Gallery Mode Emission from Dye-Doped Polymer Fiber Cross-sections** 2 **Fabricated by Near-Field Electrospinning**

3

4 Joseph E. Cheeney,<sup>a,‡</sup> Stephen T. Hsieh,<sup>a,‡</sup> Nosang V. Myung,<sup>b</sup> and Elaine D. Haberer<sup>\*,a,c</sup>5 <sup>a</sup>Materials Science and Engineering Program, University of California, Riverside, CA 925216 <sup>b</sup>Department of Chemical and Environmental Engineering, University of California, Riverside, CA 925217 <sup>c</sup>Department of Electrical and Computer Engineering, University of California, Riverside, CA 925218 <sup>\*</sup>Corresponding author email: [haberer@ucr.edu](mailto:haberer@ucr.edu)

9

---

10 **ABSTRACT:** Whispering gallery mode (WGM) resonators demonstrate great potential for photonic and sensing  
11 applications. Yet, these devices are often disadvantaged by costly materials or complex fabrication approaches, in addition  
12 to lack of manufacturing scalability. Near-field electrospinning (NFES), a recently emerged facile fiber fabrication method,  
13 offers a solution. Here, WGM resonances are reported in Rhodamine 6G-doped poly(vinyl) alcohol (PVA) microfibers via  
14 NFES. Diameters are tuned over a range of more than 10  $\mu\text{m}$  by varying substrate stage speed. Fibers display uniform  
15 distribution of dye, smooth surfaces, and circular cross-sections, all critical for supporting WGMs. High quality (Q)  
16 resonances are confirmed within fiber cross-sections through polarization experiments, free-spectral range analysis, and  
17 Mie-theory-derived mode assignment. In addition to WGMs, groups of associated spiral or conical modes are observed due  
18 to taper-induced weak optical confinement along the fiber axis. Crosslinked, dye-doped PVA fibers are utilized to sense the  
19 ethanol concentration in ethanol-water mixtures and actuation mechanisms are evaluated by comparison to theoretical  
20 spectra. The demonstration of high-Q resonances within NFES polymer microfibers is a critical step toward simple, cost  
21 effective, high-volume fabrication of WGM resonators for optoelectronics and biomedical devices.

---

## 22 **1. Introduction**

23 Among the highest quality (Q) optical cavities, whispering gallery mode (WGM) resonators have  
24 unique potential to address critical challenges in both optoelectronics and healthcare. These  
25 mirrorless structures display strong optical confinement due to total internal reflection at the  
26 cavity periphery. Their radial symmetry allows light to recirculate numerous times, enabling  
27 enhanced light-matter interactions. WGM resonances are essential to many important photonic  
28 devices including low-threshold lasers,<sup>1-5</sup> frequency combs,<sup>6-8</sup> and waveguides<sup>9</sup> as well as in  
29 sensing applications such as bulk chemical sensors,<sup>4,10-14</sup> label-free biosensors,<sup>15-17</sup> single ion  
30 detectors,<sup>18</sup> and mechanical deformation indicators.<sup>19-21</sup>

31 A wide variety of materials including glass,<sup>15,22,23</sup> semiconductors,<sup>24-29</sup> and  
32 polymers<sup>1,2,30,31</sup> have been used to make WGM resonators. Among these, polymer-based WGM

1 cavities offer reduced material costs, simple processing strategies, and straightforward  
2 incorporation of a variety of emitters. A range of polymer cavity geometries and fabrication  
3 techniques have been explored from drop casted spheres<sup>31</sup> to lithographically-defined conical  
4 structures<sup>2</sup> to inkjet-printed, wedge-shaped microdisks.<sup>32</sup> Of the many reports of WGM polymer  
5 cavities, only a limited number focus on fibers. Hollow fiber resonators have been fabricated  
6 from dye-doped polymethylmethacrylate (PMMA) preforms using heat drawing. These free-  
7 standing polymer fibers, which were 100s of microns in diameter, demonstrated both directional  
8 emission<sup>33</sup> and thermo-optic tuning of WGMs.<sup>34</sup> In addition, PMMA/epoxy resin fibers have  
9 been manually drawn directly from solution using a sharp metal tip to create WGM microlasers  
10 and refractive index based optical sensors.<sup>1,6</sup> Furthermore, arrays of PMMA/epoxy resin  
11 microfibers, embedded in PDMS were produced via spiral drawing.<sup>35</sup> In this process, the  
12 substrate served as a spool that rotated and translated via precise motor control. These dye-doped  
13 polymer fiber lasers exhibited sensitivity to strain and force perturbations. While these polymer  
14 fiber processing methods are comparatively simple and inexpensive, they lack manufacturing  
15 scalability.

16 One promising technique for high-volume, rapid manufacturing of polymer fiber WGM  
17 cavities is electrospinning, also known as far-field electrospinning. This method can be used to  
18 fabricate diverse morphologies and structures including simple homogeneous, bead-like, porous,  
19 hollow, and coaxial core-shell polymer fibers, among others.<sup>36</sup> A straightforward apparatus  
20 pumps a polymer solution through a hypodermic needle typically positioned 10s of centimeters  
21 from the substrate (or collector). A voltage applied between the needle tip and collector draws the  
22 solution from the needle, forming a liquid jet and depositing fibers on the collector with an  
23 unstable, whipping motion. Far-field electrospinning has been used to fabricate a handful of  
24 optically active resonators used as lasers<sup>37-40</sup> and organic solvent vapor sensors.<sup>41</sup> Reports

1 include dye-doped polymer fibers which support Fabry-Perot modes along their length<sup>39</sup> and 3-D  
2 resonances within their non-circular cross-sections.<sup>37</sup> In addition, ring resonators with sub-  
3 wavelength cross-sections<sup>38,41</sup> have been formed from random networks of electrospun nanofibers  
4 and bottle micro-resonators have been generated from microdroplets of polymer gain medium  
5 deposited on electrospun fibers.<sup>40</sup> While far-field electrospinning can rapidly produce many  
6 fibers, because the chaotic whipping motion far from the needle tip dominates fiber deposition it  
7 lacks the spatial precision necessary for many applications. Recently, a similar technique known  
8 as near-field electrospinning (NFES) has emerged.<sup>42</sup> This electric-field-driven approach combines  
9 the production scale of electrospinning with direct-write patterning by reducing the tip-to-  
10 collector distance from 10s of centimeters to a few millimeters or less. The lower tip-to-collector  
11 distance uses the straight, stable jet that forms near the tip, avoiding the instabilities and whipping  
12 which occur at greater distances. Notably, NFES has demonstrated the precision and control  
13 required to fabricate well-organized fiber meshes,<sup>43</sup> as well as to suspend fibers between posts  
14 just a few tens of microns in diameter.<sup>44</sup> Typically, the polymer fibers produced by NFES are  
15 approximately 10s to 100s of nanometers in diameter, too small to support high quality WGMs  
16 within their cross-sections.

17 In this work, we investigated NFES of micron-scale, dye-doped poly(vinyl) alcohol (PVA)  
18 fibers, and the high Q optical resonances supported by their smooth, circular cross-sections. PVA  
19 is a versatile water-soluble polymer which has been used in textile, biomedical and optical  
20 applications.<sup>45-47</sup> For aqueous-based applications, it can be crosslinked to form an insoluble  
21 hydrogel.<sup>48,49</sup> Sizeable weight percent solutions of PVA were used in conjunction with reduced  
22 stage speeds to direct write suspended fibers approximately 3 to 18  $\mu\text{m}$  in diameter. The  
23 emission from these slightly tapered, optically active resonators revealed groups of sharp peaks  
24 ascribed to a combination of WGMs and spiral or conical modes. The longest wavelength peak

1 within each group was identified as an in-plane WGM using mode polarization, Mie theory-based  
2 mode assignment, and free spectral range (FSR) measurements over a range of diameters. WGM  
3 quality factors of nearly 14,200 were observed for larger fiber diameters. These water-soluble  
4 PVA fibers were subsequently crosslinked via glutaraldehyde to impart stability and preserve  
5 cavity geometry for aqueous-based sensing. As a result, the maximum measured WGM cavity Q  
6 increased to approximately 19,800. As a model analyte system, the fibers were submerged in a  
7 range of ethanol-water mixtures and the corresponding WGM resonance shifts were measured as  
8 ethanol concentration was increased. Theoretical spectra were used to investigate sensing  
9 mechanisms by estimating the changes in fiber diameter and optical mode effective refractive  
10 index associated with the observed wavelength shifts. The success of NFES, a potentially low-  
11 cost, large-scale manufacturing technique, in producing micron-sized fibers that support WGMs  
12 and are highly sensitive to environmental changes is an important step toward the scalable  
13 production of affordable chemical sensors and biosensors.

## 14 **2. Experimental Details**

### 15 **2.1 Fabrication and Characterization of Electrospun Polymer Fibers**

16 PVA ( $M_w$ : 13,000-23,000 g mol<sup>-1</sup>, 98% hydrolyzed, Sigma Aldrich) and Rhodamine 6G (R6G,  
17 Sigma Aldrich) were dissolved in deionized water and mixed with a magnetic stir bar in a hot  
18 water bath at 80°C for 2 h to obtain a homogeneous 25 wt%, 0.0035 gPVA/gR6G solution. The  
19 mixture was cooled for 1 h under ambient conditions and physicochemical properties were  
20 measured including viscosity (LV DV-I Prime, Brookfield), surface tension (DuNouy Interfacial  
21 Tensiometer, Central Scientific Co. Inc.), and conductivity probe (Vernier). Optical absorbance  
22 (Cary 500, Varian), fluorescence (QM-400, Horiba), and ellipsometry (UVISEL Spectroscopic)

1 measurements were performed on spin coated thin films of the PVA/R6G solution. Ellipsometry  
2 was carried out at  $45 \pm 5\%$  humidity.

3           The dye-doped polymer solution was loaded into a 1 mL syringe and pumped through a  
4 27-gauge blunt-tip needle at a rate of  $10 \mu\text{L h}^{-1}$  using a syringe pump (NE-1010, New Era). A  
5 high voltage source (NO3.5HP8.5, Acopian) was used to apply a 2 kV to the needle tip. A glass  
6 substrate of dimensions 15 x 15 x 1 mm was used as the collector and was placed on top of an X-  
7 Y stage (A-LSQ300D, Zaber) programmed to move in a parallel-line pattern. The substrate was  
8 scribed with lines perpendicular to the intended fiber deposition direction to allow fibers to be  
9 suspended. Approximately 1 cm long fibers were written  $200 \mu\text{m}$  apart from each other. The  
10 needle tip-to-collector (T-t-C) distance was fixed at 1.25 mm, while the stage speed was varied  
11 from  $0.1\text{-}10 \text{ mm s}^{-1}$ . Electrospinning occurred under ambient temperature, pressure, and  
12 humidity. Electrospun fiber diameters were characterized using a digital optical microscope (KH-  
13 7700, Hirox) with a 35x objective and built-in measurement software. Fiber surface roughness  
14 was measured using tapping mode atomic force microscopy (AFM, Dimension Edge, Bruker) and  
15 a silicon tip. For cross-sectioning, the ends of the fibers were glued to the substrate, immersed in  
16 liquid nitrogen, and the substrate was broken along a scribe mark. While still in liquid nitrogen,  
17 the samples were placed in a vacuum desiccator for 24 h to prevent condensation from forming  
18 on the fibers. For use in scanning electron microscope (SEM; Vega3, Tescan), fibers were coated  
19 with a thin gold layer prior to characterization of fiber morphology, surfaces, and cross-sections.  
20 Confocal fluorescence microscopy (SP5, Leica Microsystems) was also used to image the dye-  
21 doped fibers.

## 22 **2.2 Crosslinking Fibers**

1 For aqueous applications, the water-soluble PVA fibers were chemically crosslinked with  
2 glutaraldehyde to make them water-stable. A three-step process, derived from previous reports,  
3 was used to crosslink the PVA fibers while still maintaining the ability to support WGMs.<sup>50,51</sup>  
4 Briefly, the fiber ends were glued to the substrate, placed in a closed chamber, and  
5 simultaneously exposed to vapor from a 1 M HCl solution and a 50% glutaraldehyde solution for  
6 24 h. Next, the fibers were exposed to vapor from a 5 M HCl solution and a 50% glutaraldehyde  
7 solution for 24 h. For the last step, the fibers were submerged in a 50% glutaraldehyde solution  
8 for 24 h, rinsed thoroughly with water, and allowed to dry.

### 9 **2.3 Optical WGM Measurement and Sensing**

10 A laser confocal system (LabRam, Horiba Scientific) in a microphotoluminescence ( $\mu\text{PL}$ )  
11 configuration was used to evaluate the dye-doped PVA fiber WGM resonators. A single fiber was  
12 optically excited with 1  $\mu\text{W}$  from a 532 nm CW laser (Ventus, Laser Quantum) focused to a spot  
13 size of approximately 3  $\mu\text{m}$  using a 50x objective ( $\text{NA} = 0.75$ ). Resonator emission was collected  
14 with the same objective, directed through a longpass filter ( $> 532$  nm), and analyzed using a  
15 charge-coupled device (CCD) spectrometer with an 1800 lines  $\text{mm}^{-1}$  grating and a spectral  
16 increment of around 0.014 nm. WGM Q factors were analyzed by fitting each peak with a  
17 Lorentzian function. For ethanol-water sensing experiments, the sample was submerged in a pool  
18 of water in which the ethanol concentration was varied from 0 to 30% by volume while keeping  
19 the total solution volume constant. Spectra were collected in 3 min intervals. The laser was  
20 shuttered between measurements to prevent photothermal effects and minimize bleaching. A 50x  
21 long-working-distance ( $\text{NA} = 0.50$ ) objective was used, and the excitation power was increased  
22 to 2  $\mu\text{W}$ .

1 To determine important WGM parameters and azimuthal mode numbers, theoretical  
 2 spectra were obtained by using a Mie-theory derived approximation<sup>52</sup>

$$3 \quad \lambda \cong \pi n_{host} D \left[ v + \frac{\alpha_s v^{\frac{1}{3}}}{2^{\frac{1}{3}}} - \frac{P}{(n_{eff}^2 - 1)^{\frac{1}{2}}} + \frac{3}{10} \frac{\alpha_s^2}{2^{\frac{2}{3}} v^{\frac{1}{3}}} - \frac{P(n_{eff}^2 - \frac{2P}{3})}{(n_{eff}^2 - 1)^{\frac{3}{2}}} \frac{\alpha_s}{2^{\frac{1}{3}} v^{\frac{2}{3}}} \right]^{-1} \quad (1)$$

4 where  $D$  is resonator diameter,  $v$  is the mode number + 0.5,  $\alpha_s$  are the roots of the Airy function,  
 5  $n_{eff}$  is the effective refractive index of the resonance, and  $P = 1/n_{eff}$  for TM and  $n_{eff}$  for TE modes,  
 6 respectively. The refractive index of the surrounding medium ( $n_{host}$ ) was taken as either 1.000 for  
 7 fibers in air or was based on literature measurements for ethanol-water concentrations<sup>53</sup> (shown in  
 8 Figure S1), with values ranging from 1.3325 to 1.3494. Equation (1) was evaluated by  
 9 incrementally varying  $D$ ,  $n_{eff}$  and azimuthal mode number. Solutions were compared to  
 10 fluorescence spectra obtained from the WGM fibers, and the least mean residual squared was  
 11 taken as the best fit. The range of input  $D$  and  $n_{eff}$  values used to determine best fit corresponded  
 12 to optical images and ellipsometry measurements, respectively. For sensing of ethanol-water  
 13 mixtures, measurements made within 5 min of ethanol addition were disregarded due to transient  
 14 behavior and the mode number was constrained despite changing ethanol-water concentrations.

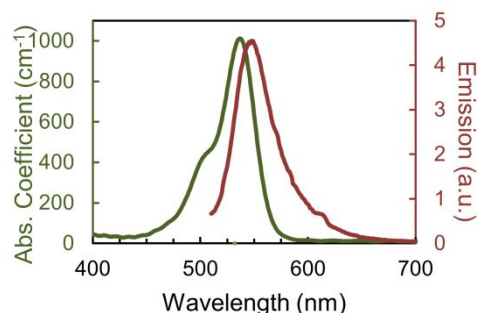
### 15 **3. Results and Discussion**

#### 16 **3.1 Near-Field Electrospinning of Dye-Doped Polymer Fiber Resonators**

17 Solutions for NFES of optically active, fiber resonators were prepared by combining R6G with  
 18 PVA. A relatively high weight percent PVA was used to spin fibers. Typically, increasing  
 19 polymer weight percent increases viscosity and conductivity while reducing surface tension, all of  
 20 which contribute to the fabrication of larger fibers.<sup>36,54</sup> Because they are critical in manipulating  
 21 electrospun fiber diameter, the physicochemical properties of these solutions were measured. The



1 surface tension, electrical conductivity, and viscosity were  $56 \pm 1$  dynes  $\text{cm}^{-1}$ ,  $2726 \pm 102$   $\mu\text{S cm}^{-1}$ ,  
2  $^1$ , and  $717.5 \pm 73.8$  cP, respectively. For the purpose of optical characterization, this dye-doped  
3 polymer solution was spin-coated onto a glass slide, forming an approximately  $5 \mu\text{m}$  thick film.  
4 The absorbance and emission spectra of the R6G-PVA film were measured and are shown in  
5 Figure 1. Peak absorbance and emission wavelengths were 537 nm and 548 nm, respectively.  
6 Minimal spectral overlap of absorbance and emission was observed for wavelengths greater than  
7 575 nm. As measured by ellipsometry at  $45 \pm 5\%$  humidity, the average refractive index,  $n$ , of  
8 the R6G-PVA films between 580 and 700 nm was  $n = 1.464 \pm 0.006$ .



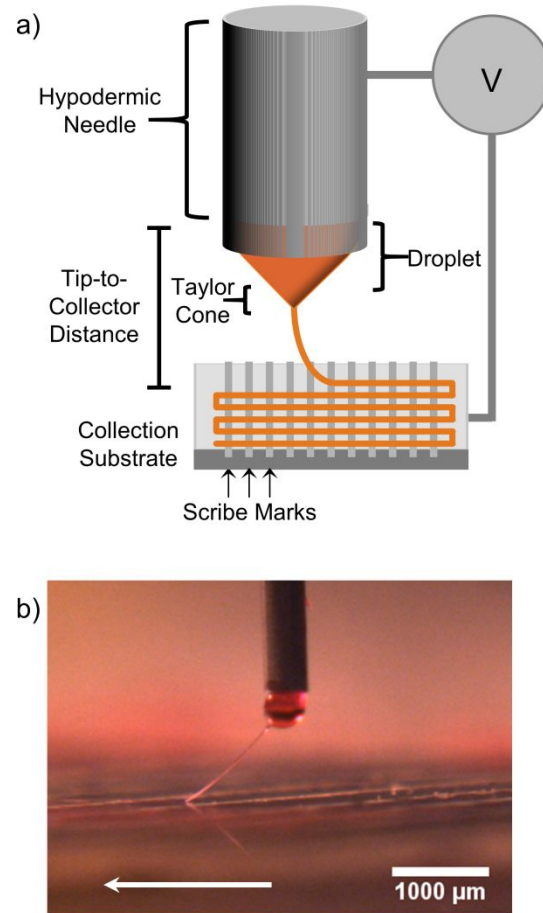
9

10 Figure 1. Absorption and emission spectra of spin-coated R6G-PVA thin film.

11

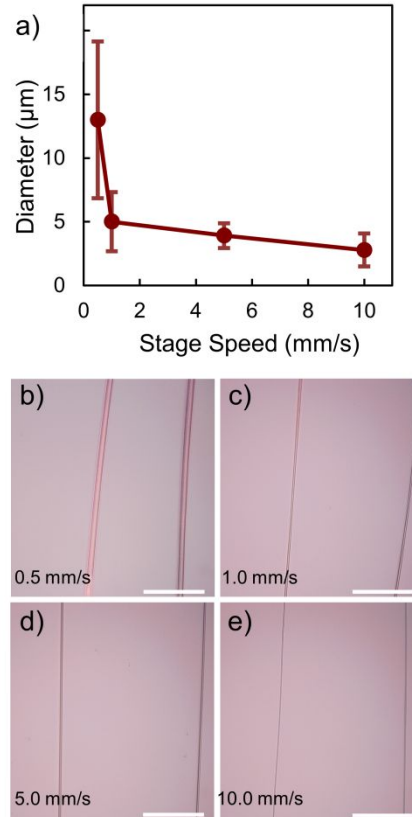
12 The NFES system used to fabricate fiber-based optical cavities is illustrated in Figure 2a.  
13 The polymer solution was pumped through a syringe and fed through a hypodermic needle,  
14 forming a droplet. An applied voltage between the needle (tip) and substrate (collector) allowed  
15 the polymer solution to overcome its surface tension, generate a Taylor cone, and induce fiber  
16 formation. Fiber was deposited on the collection substrate as the computer-controlled stage  
17 scanned in a programmed parallel-line pattern composed of lines 1 cm in length, spaced  
18 approximately  $200 \mu\text{m}$  apart. With these dimensions, 10s of fibers were written on a single  
19 substrate. Electrospinning of the R6G-PVA solution is depicted in Figure 2b. Microscale polymer

1 fiber was drawn from the droplet in the scan direction. As shown in Figure 3a, fiber diameter was  
2 dependent on stage speed. Optical images of fibers for each electrospinning condition, in addition  
3 to histograms of fiber diameter, are shown in Figures 3b-e and S2, respectively. Using a scan rate  
4 of  $10 \text{ mm s}^{-1}$  the average fiber diameter was  $2.8 \pm 1.3 \text{ }\mu\text{m}$ , whereas a reduced stage speed of  $0.5$   
5  $\text{mm s}^{-1}$  increased the average diameter to  $12.4 \pm 5.9 \text{ }\mu\text{m}$ . Thus, average fiber size was adjusted by  
6 more than a factor of 4. Scan velocity can control the degree of mechanical drawing of the  
7 polymer solution during spinning, greatly influencing fiber diameter.<sup>44,55</sup> Similar trends have also  
8 been observed for stage speeds 2 to 40 times larger than used in these studies.<sup>44,55-57</sup> The  
9 combination of electrospinning parameters (e.g. solution, pattern dimensions, etc.) used here  
10 approached the spatial limitations of our apparatus and controller. As a result, scan rate affected  
11 pattern fidelity with write deviations increasing at higher speeds, particularly near end points. The  
12 use of rather viscous, high weight percent polymer solution and reduced stage speed enabled  
13 fabrication of larger fibers. The sizable diameters generated by a  $0.5 \text{ mm s}^{-1}$  stage speed were  
14 compatible with observation of high quality WGMs, therefore fibers electrospun with these  
15 conditions were selected for further study.



1

2 Figure 2. a) Schematic of near-field electrospinning (NFES) apparatus showing deposition of  
3 suspended polymer microfibers. b) Optical image of Taylor cone formation and fiber drawing  
4 from polymer droplet during NFES process. The arrow indicates the direction of stage motion.



1

2 Figure 3. R6G-PVA electrospun fiber a) diameter and b)-e) optical images as a function of stage  
 3 speed. Average fiber diameter increased as scan rate decreased. Average and standard deviation  
 4 were determined from >85 measurements. Scale bars: 100 μm.

5

6 Using a scan rate of 0.5 mm s<sup>-1</sup>, R6G-PVA fibers were electrospun on a glass substrate.

7 Prior to electrospinning, 5-10 scribe marks were made in the substrate perpendicular to the fiber

8 deposition direction as previously indicated in Figure 2a. These nearly 20 μm deep trenches

9 prevented optical coupling of resonator-supported-modes to the underlying glass substrate. Figure

10 4a and 4b show the fluorescence emission and an SEM image of electrospun dye-doped polymer

11 fibers suspended across a scribe mark, respectively. R6G fluorescence was relatively uniform

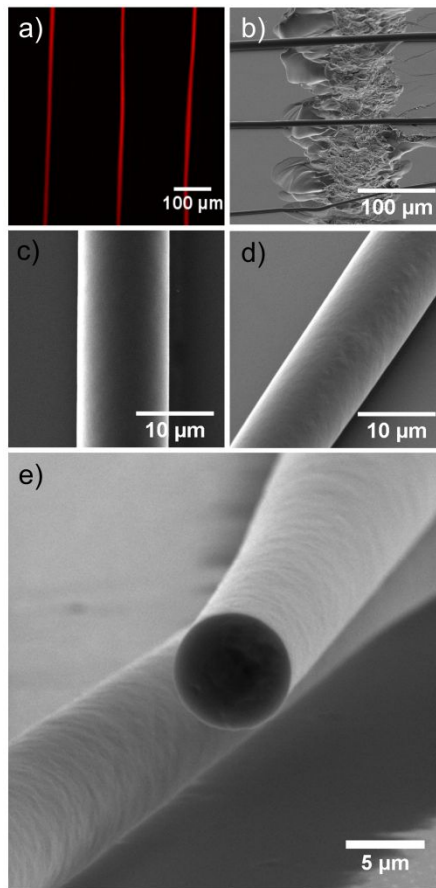
12 throughout the fibers, without evidence of substantial dye molecule agglomeration. In addition,

13 no fiber sagging or drooping was observed. Higher magnification electron microscope images,

14 shown in Figure 4c and 4d, revealed smooth fiber surfaces without significant striations or ridges.

1 A root-mean-squared roughness of 2.4 nm was measured via atomic force microscopy (Figure  
2 S3). Moreover, fiber cross-sections produced with the freeze-snap technique were circular, and  
3 void of flat regions or significant distortions in shape, as shown in Figure 4e. These fibers were  
4 an enhancement upon a previous report of similarly sized electrospun polymer fiber resonators  
5 which yielded rough, non-circular structures.<sup>37</sup> As revealed in Figure S4, fiber diameter was  
6 found to vary gradually with length, and no bead-like structures were observed. More than 15  
7 fibers, with over 200  $\mu\text{m}$  in length analyzed on each, indicated an average diameter change of  
8  $0.037 \pm 0.034 \mu\text{m}$  per micron of fiber length.

9



10

11 Figure 4. a) Fluorescent emission and b-e) representative SEM images of PVA fibers electrospun  
12 with a stage speed of  $0.5 \text{ mm s}^{-1}$  and a R6G/PVA mass ratio of 0.0035.

1

2 **3.2 Whispering Gallery Mode Detection and Characterization**

3 Emission from the R6G-PVA fiber optical cavities was measured using a  $\mu$ PL set-up with a  
4 coherent, continuous wave (CW) 532 nm excitation source and an approximately 3  $\mu$ m spot size.

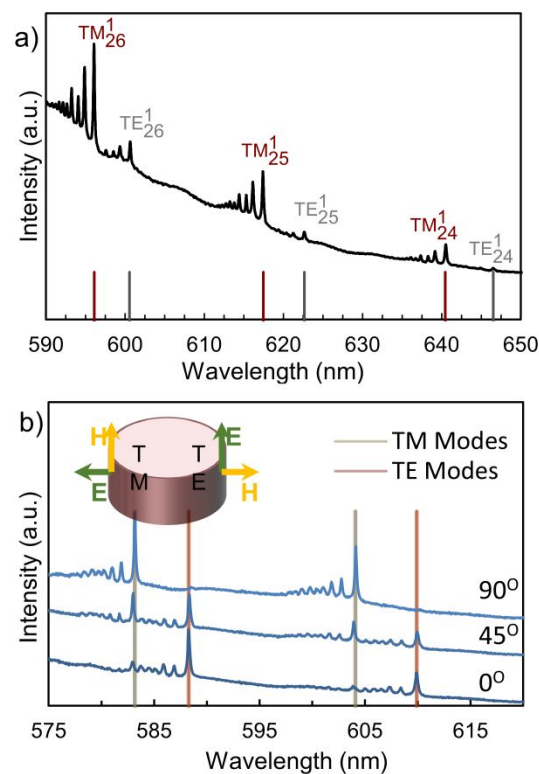
5 Excitation power dependent measurements from 5 nW to 50  $\mu$ W indicated that the resonators  
6 were in the spontaneous emission regime. The higher excitation power failed to produce lasing,  
7 likely due to the insufficient photostability of fluorescent dye.<sup>58</sup> Consequently, to minimize dye  
8 bleaching, yet ensure an adequate signal-to-noise ratio, 1  $\mu$ W of excitation power was used.

9 Figure 5a shows a representative spectrum of a single, as-spun dye-doped PVA fiber with a  
10 measured diameter of 4.2  $\mu$ m. The investigation focused on wavelengths greater than 575 nm due  
11 to the minimal overlap in R6G absorbance and emission within this spectral region. Paired groups  
12 of sharp resonances were observed to decorate the broad fluorescence emission of R6G. The  
13 WGM resonance condition is:

$$14 \quad m\lambda = \pi D n_{eff} \quad (2)$$

15 where  $m$  is an integer,  $\lambda$  is the wavelength,  $D$  is the resonator diameter, and  $n_{eff}$  is the effective  
16 refractive index. The groups of closely spaced modes were attributed to WGMs supported within  
17 the fiber cross-section, in addition to spiral or conical modes with finite longitudinal components  
18 and wavelengths slightly smaller than WGM resonance.<sup>59–61</sup> Variations in fiber geometry  
19 including both bottle structures<sup>62,63</sup> and tapers<sup>64,65</sup> can facilitate the observed optical confinement.  
20 In particular, the aforementioned diameter changes were likely contributors. To further  
21 investigate the groups of closely spaced modes, emission was collected along the length of the  
22 fiber in 0.8  $\mu$ m increments (Figure S4). Within each spectrum, the dominant intensity peak was  
23 dependent on measurement location. As the excitation and collection optic was scanned along the

1 fiber length, resonance features emerged and faded within a short distance, typically  $< 10 \mu\text{m}$ ,  
 2 indicating fairly compact mode localization. Previous reports<sup>59,60</sup> attribute this form of mode  
 3 localization to conically-shaped fibers that confine light via a reflection process on the smaller  
 4 diameter side and a self-interference process on the larger diameter side. Additional  
 5 electrospinning process development is required to more precisely control fiber diameter, and  
 6 further suppress longitudinal resonance components.



7  
 8 Figure 5. a) Spectrum of 4.2  $\mu\text{m}$  diameter dye-doped, electrospun PVA fiber. Broad fluorescence  
 9 emission was decorated by groups of sharp peaks. Mie theory was used to identify first order TE  
 10 and TM WGMs. b) Spectra of a 4.7  $\mu\text{m}$  diameter fiber taken with a polarizing filter to establish  
 11 the polarization of the resonances. At  $0^\circ$  the polarizer is parallel to fiber axis while at  $90^\circ$  the  
 12 polarizer is perpendicular. Inset: E and H field vector orientation associated with TM and TE  
 13 modes.

14

1 To distinguish modes with similar electromagnetic field oscillation, a polarizer was placed  
 2 between the fiber and the monochromator. Representative polarization-dependent spectra are  
 3 shown in Figure 5b. Here, modes with the electric field vector perpendicular to the resonator  
 4 surface are transverse magnetic (TM) and modes with the electric field vector parallel to the  
 5 length of the fiber are transverse electric (TE). As demonstrated, within a group, all the peaks  
 6 were the same polarization. The shorter and longer wavelength groups were TM and TE,  
 7 respectively.

8 Having identified the peak pairs as TE and TM WGM modes, theoretical spectra were  
 9 calculated using an asymptotic formula for resonance and mode identification based on Mie  
 10 theory.<sup>52</sup> The position of the highest intensity peak within each group was compared to the  
 11 corresponding theoretical peak value, and the best fit was determined by the least sum of the  
 12 residuals squared. Resonances were assumed to be first order radial WGMs, as these are typically  
 13 the lowest loss modes. Mode assignments in Figure 5a correspond to a diameter of 4.5  $\mu\text{m}$  and  
 14  $n_{eff}$  of 1.3080 (TE) and 1.239 (TM). Because TM and TE modes penetrate the surrounding  
 15 environment to different degrees, a small difference in  $n_{eff}$  values was expected.

16 As illustrated in Figure 6a, the longest wavelength peaks, associated with in-plane WGM  
 17 resonances, from two successive groups within the same polarization were used to determine free  
 18 spectral range (FSR). The spacing between consecutive modes was expected to decrease with  
 19 increasing cavity length as defined by:

$$20 \quad FSR = \frac{\lambda^2}{Ln_{eff}} \quad (3)$$

21 where  $L$  is the resonator path length. For WGMs, the cavity circumference,  $\pi D$ , is nominally the  
 22 path length. FSR is plotted versus fiber diameter in Figure 6b for dye-doped electrospun fibers



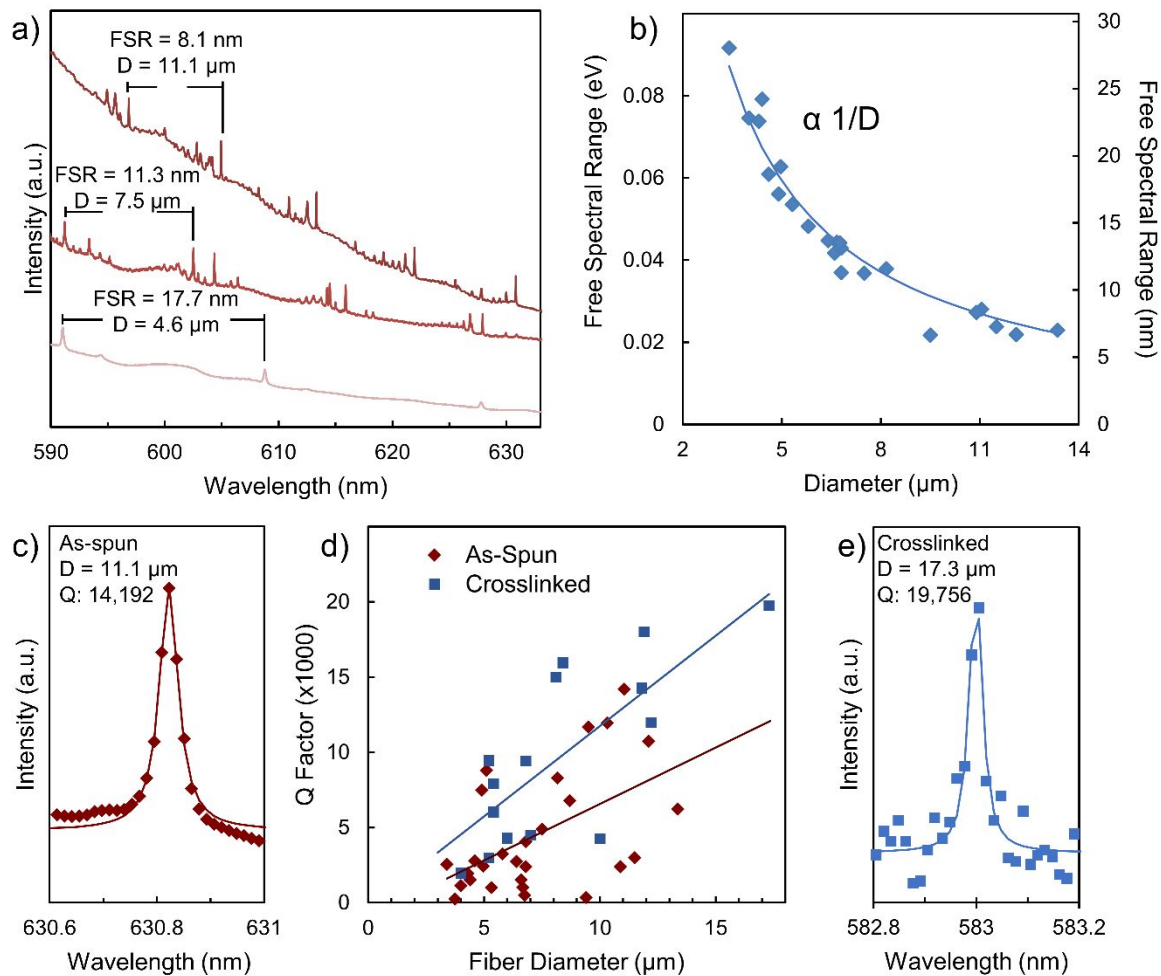
1 ranging from 3 to 18  $\mu\text{m}$  in size. The inverse relationship between FSR and  $D$  (as emphasized by  
2 the solid curve), is characteristic of WGMs and further excludes both Fabry-Perot resonances<sup>37</sup>  
3 along the fiber length and random cavity resonances.<sup>38,39</sup> Cavity Q-factors, defined as:

$$4 \quad Q = \frac{\lambda_{\text{Resonance}}}{\lambda_{\text{FWHM}}} \quad (4)$$

5 were evaluated for several optical cavities by fitting each peak with a Lorentzian function. A  
6 single high Q peak ( $\sim 14,200$ ) with a 0.044 nm FWHM is represented in Figure 6c and measured  
7 Q values for a range of as-spun fiber diameters are shown in Figure 6d. Given the relatively  
8 weak dependence of Q factor on diameter, radiative losses were not dominant, but rather material  
9 absorption or surface scattering were considered the main limitations on resonator  
10 performance.<sup>66-68</sup> Compared to other similarly sized polymer fibers, the near-field electrospun  
11 WGM fiber resonators described here possessed higher Q-factors. As example,  $\sim 10 \mu\text{m}$  diameter  
12 manually drawn dye-doped PMMA/epoxy fibers have been reported with Q-factors near 6500<sup>1</sup>.  
13 Similarly, a Q-factor of 1942 has been measured for an 11.7  $\mu\text{m}$  far-field electrospun dye-doped  
14 PMMA fiber<sup>69</sup>. Notably, unlike the WGM fiber resonators studied here, both reports were under  
15 lasing or hot cavity conditions with significant linewidth narrowing.

16

17



1  
2 Figure 6. a) Emission spectra of three different fiber diameters with free spectral range (FSR)  
3 measured between the longest wavelength peaks from successive groups within the same  
4 polarization. Emission intensity is offset for clarity. b) FSR plotted as a function of fiber  
5 diameter. FSR was proportional to  $1/D$  as denoted by the solid line. c) A high Q mode associated  
6 with the as-spun 11.1  $\mu\text{m}$  diameter fiber in part a) with a Lorentzian curve fit. d) Q-factor plotted  
7 versus diameter for as-spun and crosslinked fibers. Q values approaching 14,200 for as-spun  
8 fibers and nearly 19,800 for crosslinked fibers were recorded for larger diameters. e) A high Q  
9 mode associated with a 17.3  $\mu\text{m}$  diameter crosslinked fiber with a Lorentzian curve fit.

10

11 A three-step glutaraldehyde treatment based, in part, on previous reports<sup>50,51</sup> was used to  
12 crosslink dye-doped PVA fibers, rendering them insoluble in aqueous solution. As shown in  
13 Figure S6, after crosslinking, there was an approximately 13% increase in average fiber diameter  
14 and some fiber curvature developed (Figure 7a). This was likely due to swelling and/or polymer

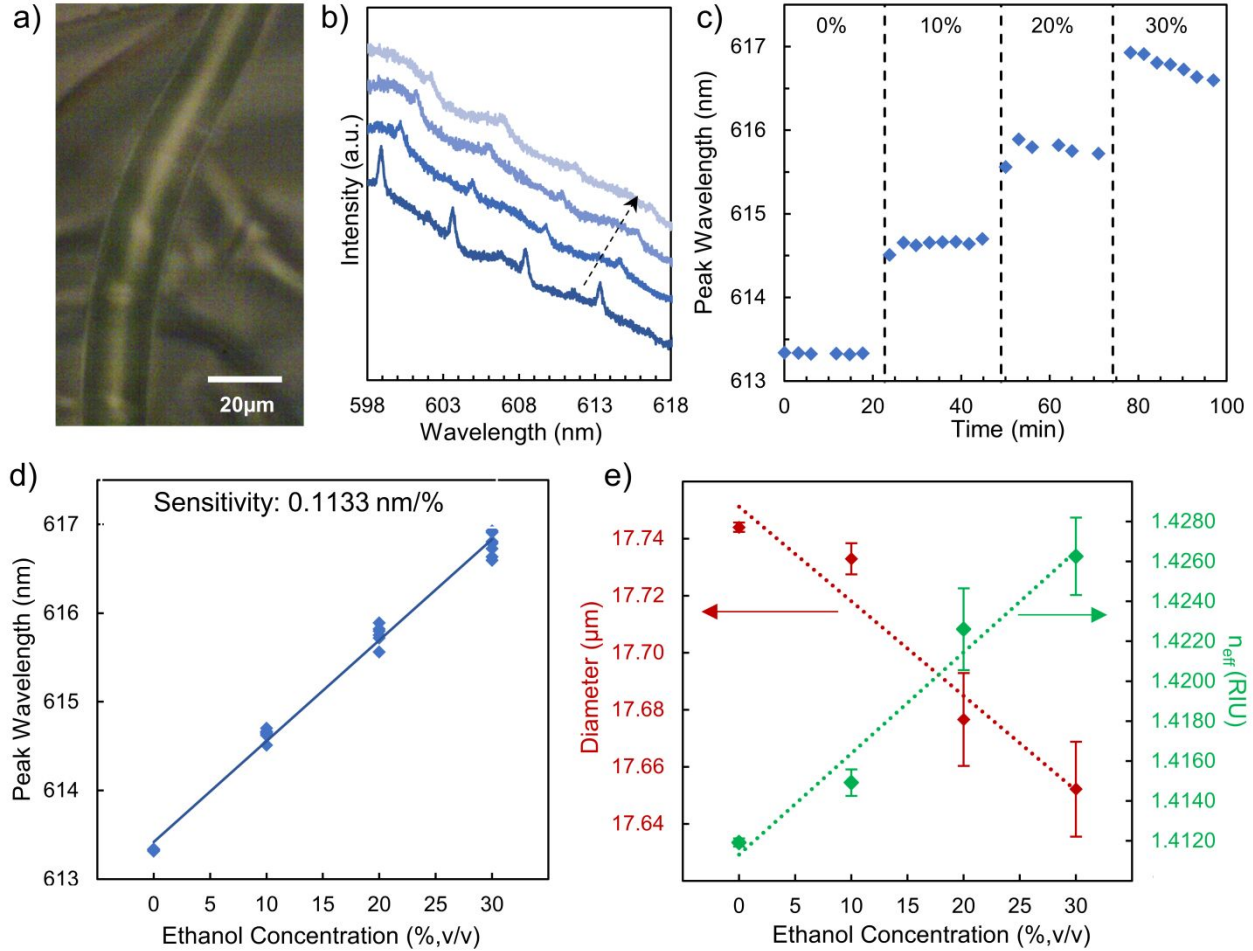
1 relaxation associated with the water-based crosslinking process. Nonetheless, as demonstrated in  
2 Figure S7, after immersion in water for 24 h, glutaraldehyde-treated PVA fibers were unchanged  
3 and no additional swelling or distortion in shape was observed. The photoluminescence of the  
4 crosslinked fibers was measured in air. As described in Figure 6d and 6e, after glutaraldehyde  
5 treatment, Q factors increased overall, attaining a value near 19,800 for one of the larger diameter  
6 fibers. Further studies are necessary to fully understand this phenomena, but it is believed that the  
7 crosslinking process may reduce fiber surface roughness and the associated scattering losses via  
8 solvent-vapor surface smoothing.<sup>70</sup>

### 9 **3.3 Ethanol-Water Sensing**

10 WGM resonators have shown great utility as chemical and biological sensors.<sup>1,6,15</sup> Electrospun  
11 R6G-PVA micro-fibers were assessed as chemical sensors using ethanol in water as a model  
12 system. A crosslinked WGM fiber resonator was placed in a water bath, as in Figure 7a, and  
13 optical spectra were collected. Notably, once submerged, resonance wavelengths were invariant  
14 in the water bath (Figure S8), thus supporting optical microscopy evidence that the crosslinked  
15 PVA fibers were water stable, and that heating effects were minimal. Q values of the submerged  
16 fibers shrunk by roughly a factor of 9 and FSR decreased slightly due to the sizable reduction in  
17 refractive index difference between the cavity and its surroundings. For ethanol-water sensing,  
18 the concentration of ethanol was increased in 10% (v/v) increments. As shown in Figure 7b, a  
19 corresponding red-shift in WGMs resonant wavelength was associated with each increase. The  
20 resonant wavelength of the mode initially observed at 613.5 nm was plotted as a function of time  
21 in Figure 7c. Immediately after each addition of ethanol, the resonant wavelength rapidly  
22 increased, and then plateaued. Evaporation losses at higher ethanol concentrations resulted in  
23 small, but discernable blue shifts at longer measurement times. Figure 7d depicts the resonance

1 wavelength of the same peak versus ethanol concentration. The spectral response of the resonator  
2 was linear within the range of ethanol concentrations measured, resulting in a sensitivity of  
3 0.1133 nm/%. As demonstrated in Figure S9, the sensitivity of the cavity to ethanol  
4 concentration was wavelength dependent, due to decreased light confinement at longer  
5 wavelengths. Using the relationship between refractive index and ethanol concentration found in  
6 Figure S1<sup>53</sup>, the measured sensitivities were comparable to those of other polymer-based WGM  
7 resonators. As an example, dye-doped PMMA/epoxy resin fibers<sup>6</sup> had a sensitivity of  
8 approximately 0.1391 nm/%. Similarly, hollow PMMA fibers embedded with a dye-doped  
9 microrings<sup>71</sup> demonstrated sensitivities near 0.1245 nm/%.

10



1  
 2 Figure 7. a) A 15.9  $\mu\text{m}$  diameter WGM fiber sensor submerged in a water bath. b) Fluorescence  
 3 spectra of fiber resonator in 0%, 10%, 20%, and 30% (v/v) ethanol-water solution. Arrow  
 4 indicates increasing ethanol concentration. Emission intensities are offset for clarity. c) Peak  
 5 emission wavelength of the mode initially observed at 613.5 nm as a function of time. A red-shift  
 6 in WGM resonance was observed for each increase in ethanol concentration (as denoted by  
 7 dashed, vertical lines). d) Peak emission wavelength as a function of ethanol concentration. The  
 8 calculated sensitivity within this linear performance region was 0.1133 nm/%. e) Calculated  
 9 resonator diameters and effective refractive indices with increasing ethanol concentration; fiber  
 10 diameters shrunk slightly, while  $n_{eff}$  increased. Each data point represents the average fitted  
 11 diameter or  $n_{eff}$  obtained.

12 Both volumetric and effective refractive index changes can contribute to WGM  
 13 wavelength shifts and sensor performance. The relationship between resonance shift and these  
 14 mechanisms can be expressed by

$$15 \quad \frac{\Delta\lambda}{\lambda} = \frac{\Delta n_{eff}}{n_{eff}} + \frac{\Delta D}{D} \quad (5)$$

1 Due to the evanescent field associated with WGMs, the effective refractive index depends on  
2 both  $n_{cavity}$  and  $n_{host}$ . Unlike inorganic optical resonators, the addition of solute can cause changes  
3 in the  $n_{cavity}$  of polymer cavities through solute uptake, as well as  $n_{host}$ . Furthermore, solute  
4 uptake can be accompanied by resonator dimensional changes. Indeed, other WGM polymer-  
5 based cavities have demonstrated the combined influence of environmental refractive index,  
6 solvent uptake, and/or cavity expansion or contraction on sensor response<sup>41,72–75</sup>. When exposed  
7 to alcohol vapors, both swelling and vapor uptake caused redshifts in resonances of random  
8 optical networks of poly(methyl methacrylate) (PMMA) fibers<sup>41</sup>. Similarly, interaction of volatile  
9 organic compounds with PDMS-coated SiO<sub>x</sub> quasi-toroidal ring resonators resulted in a redshift  
10 which could be parsed in to contributions from polymer swelling and an increase in  $n_{cavity}$ <sup>74</sup>.  
11 Additionally, solvent penetration and swelling were observed for WGMs in polystyrene  
12 microbeads immersed in alcohol solutions, although changes in  $n_{host}$  dominated sensor  
13 performance<sup>75</sup>.

14 To understand the transduction mechanisms associated with the crosslinked, dye-doped  
15 PVA WGM fibers, the sensing spectra were examined using Equation (1), a Mie theory-based  
16 asymptotic formula, to extract best fit values for  $D$ ,  $n_{eff}$ , and azimuthal mode number. Similar Mie  
17 theory approaches have been used to account for dimensional and refractive index changes  
18 associated with humidity, or adsorbed polyelectrolyte and biomolecule layers<sup>73,76,77</sup>. The average  
19 best fit diameters and effective refractive indices for all sensing spectra as a function of ethanol  
20 concentration are shown in Figure 7e. As the ethanol concentration increased from 0 to 30%, the  
21 calculated  $D$  shrank approximately 90 nm or just 0.5%. The reduction in diameter is consistent  
22 with reports of highly crosslinked PVA hydrogels with a large degree of hydrolysis in ethanol-  
23 water solvent mixtures<sup>78–80</sup>. Conversely,  $n_{eff}$  increased with ethanol concentration. As the  
24 refractive index of ethanol is larger than water, depending on the extent of fiber uptake, both  $n_{host}$

1 and  $n_{cavity}$  could contribute to this increase. The resonance peak is expected to blue-shift as fiber  
2 diameter shrinks and red-shift as  $n_{eff}$  increases. As a net red-shift was observed with increasing  
3 ethanol concentration, the sensing performance of the WGM fiber was dominated by an effective  
4 refractive index change rather than dimensional change.

### 5 **3. Conclusion**

6 To conclude, NFES was used to fabricate R6G-PVA fibers that supported WGM resonances  
7 within their cross-sections. This readily scalable, direct-write technique allowed for precise,  
8 patterned deposition of several centimeters of fibers on each substrate. By utilizing a relatively  
9 high weight percent polymer solution and stage speeds much slower than other NFES  
10 reports,<sup>44,55-57</sup> fiber diameters were tuned into the micron range while maintaining smooth  
11 surfaces and circular cross-sections. The broad fluorescence emission of these fibers was  
12 decorated by groups of high Q peaks. These resonances were ascribed to WGMs which  
13 circulated around the fiber circumference, as well as spiral or conical modes with small  
14 longitudinal components and slightly smaller wavelengths. Additional studies are needed to  
15 minimize axial components and simplify the spectra of these optically active resonators. For  
16 aqueous applications, R6G-PVA fibers were crosslinked with a glutaraldehyde treatment. This  
17 process caused fiber diameters to swell and cavity Q to increase, likely due to solvent-vapor  
18 smoothing of the fiber surface. Despite emission spectrum complexity, chemical sensing of the  
19 ethanol-water system exhibited a sensitivity of 0.1133 nm/%. NFES of dye-doped polymer  
20 microfiber WGM resonators has proven promising as a straightforward, inexpensive fabrication  
21 approach. Given the variety of emitters that can easily be incorporated within NFES polymer  
22 fibers, the biocompatibility of PVA, and the spatial precision associated with the direct-write

1 technique, multiplexed WGM polymer fiber sensors capable of simultaneously detecting multiple  
2 analytes are within reach.

### 3 **4. Conflict of Interest**

4 There are no conflicts to declare.

### 5 **5. Acknowledgement**

6 This material is based upon work supported by the National Science Foundation under Grant No.  
7 ECCS-1406795 and the UCR CoR Grant Program. In addition, this study utilized the Analytical  
8 Chemistry Instrumentation Facility, the Institute for Integrative Genome Biology at UC  
9 Riverside, Winston Chung Global Energy Center and Ming Chi University of Technology.

### 10 **6. Notes and References**

- 11 1 V. Duong Ta, R. Chen, L. Ma, Y. Jun Ying and H. Dong Sun, *Laser Photonics Rev.*, 2013,  
12 7, 133–139.
- 13 2 T. Grossmann, S. Schleede, M. Hauser, M. B. Christiansen, C. Vannahme, C.  
14 Eschenbaum, S. Klinkhammer, T. Beck, J. Fuchs, G. U. Nienhaus, U. Lemmer, A.  
15 Kristensen, T. Mappes and H. Kalt, *Appl. Phys. Lett.*, 2010, **97**, 1–4.
- 16 3 Y. Wang, V. D. Ta, K. S. Leck, B. H. I. Tan, Z. Wang, T. He, C. D. Ohl, H. V. Demir and  
17 H. Sun, *Nano Lett.*, 2017, **17**, 2640–2646.
- 18 4 T. Wienhold, S. Kraemmer, S. F. Wondimu, T. Siegle, U. Bog, U. Weinzierl, S. Schmidt,  
19 H. Becker, H. Kalt, T. Mappes, S. Koeber and C. Koos, *Lab Chip*, 2015, **15**, 3800–3806.
- 20 5 X. F. Jiang, C. L. Zou, L. Wang, Q. Gong and Y. F. Xiao, *Laser Photonics Rev.*, 2016, **10**,  
21 40–61.
- 22 6 V. D. Ta, R. Chen and H. Sun, *Adv. Opt. Mater.*, 2014, **2**, 220–225.
- 23 7 H. Choi and A. M. Armani, *Opt. Lett.*, 2018, **43**, 2949–2952.
- 24 8 A. A. Savchenkov, A. B. Matsko, V. S. Ilchenko, I. Solomatine, D. Seidel and L. Maleki,  
25 *Phys. Rev. Lett.*, 2008, **101**, 093902.
- 26 9 A. A. Savchenkov, W. Liang, V. Ilchenko, A. Matsko and L. Maleki, *IEEE J. Sel. Top.*  
27 *Quantum Electron.*, 2018, **24**, 2900111.
- 28 10 R. Bischler, M. Olszyna, M. Himmelhaus and L. Dähne, *Eur. Phys. J. Spec. Top.*, 2014,  
29 **223**, 2041–2055.
- 30 11 N. M. Hanumegowda, C. J. Stica, B. C. Patel, I. White and X. Fan, *Appl. Phys. Lett.*, 2005,  
31 **87**, 201107.
- 32 12 V. Zamora, A. Díez, M. V. Andrés and B. Gimeno, *Opt. Express*, 2007, **15**, 12011–12016.
- 33 13 V. D. Ta, R. Chen and H. D. Sun, *Sci. Rep.*, 2013, **3**, 1362.
- 34 14 X. Zhang, L. Ren, X. Wu, H. Li, L. Liu and L. Xu, *Opt. Express*, 2011, **19**, 22242–22247.



- 1 15 F. Vollmer and S. Arnold, *Nat. Methods*, 2008, **5**, 591–596.
- 2 16 M. D. Baaske, M. R. Foreman and F. Vollmer, *Nat. Nanotechnol.*, 2014, **9**, 933–939.
- 3 17 F. Vollmer, S. Arnold and D. Keng, *Proc. Natl. Acad. Sci. U. S. A.*, 2008, **105**, 20701–  
4 20704.
- 5 18 M. D. Baaske and F. Vollmer, *Nat. Photonics*, 2016, **10**, 733–739.
- 6 19 T. Siegle, M. Rimmel, S. Krämmer and H. Kalt, *APL Photonics*, 2017, **2**, 096103.
- 7 20 Y. Yang, Y. Ooka, R. Thompson, J. Ward and S. N. Chormaic, *Opt. Lett.*, 2015, **41**, 8–11.
- 8 21 C. L. Linslal, M. Kailasnath, S. Mathew, T. K. Nideep, P. Radhakrishnan, V. P. N.  
9 Nampoori and C. P. G. Vallabhan, *Opt. Lett.*, 2016, **41**, 551–554.
- 10 22 G. Senthil Murugan, J. S. Wilkinson and M. N. Zervas, *Opt. Express*, 2009, **17**, 11916–  
11 11925.
- 12 23 D. Navarro-Urrios, M. Baselga, F. F. Lupi, L. L. Martín, C. Pérez-Rodríguez, V. Lavin, I.  
13 R. Martín, B. Garrido and N. E. Capuj, *J. Opt. Soc. Am. B*, 2012, **29**, 3293–3298.
- 14 24 S. Imamura, R. Watahiki, R. Miura, T. Shimada and Y. K. Kato, *Appl. Phys. Lett.*, 2013,  
15 **102**, 161102.
- 16 25 B. D. Jones, M. Oxborrow, V. N. Astratov, M. Hopkinson, A. Tahraoui, M. S. Skolnick  
17 and A. M. Fox, *Opt. InfoBase Conf. Pap.*, 2011, **18**, 3302–3307.
- 18 26 S. L. McCall, A. F. J. Levi, R. E. Slusher, S. J. Pearton and R. A. Logan, *Appl. Phys. Lett.*,  
19 1992, **60**, 289–291.
- 20 27 E. D. Haberer, R. Sharma, C. Meier, A. R. Stonas, S. Nakamura, S. P. Denbaars and E. L.  
21 Hu, *Appl. Phys. Lett.*, 2004, **85**, 5179–5181.
- 22 28 T. Kipp, H. Welsch, C. Strelow, C. Heyn and D. Heitmann, *Phys. Rev. Lett.*, 2006, **96**,  
23 077403.
- 24 29 K. Srinivasan, A. Stintz, S. Krishna and O. Painter, *Phys. Rev. B - Condens. Matter Mater.*  
25 *Phys.*, 2005, **72**, 205318.
- 26 30 A. M. Armani, A. Srinivasan and K. J. Vahala, *Nano Lett.*, 2007, **7**, 1823–1826.
- 27 31 A. François, N. Riesen, H. Ji, S. Afshar V. and T. M. Monroe, *Appl. Phys. Lett.*, 2015, **106**,  
28 031104.
- 29 32 C. Chen, L. Wan, H. Chandralalim, J. Zhou, H. Zhang, S. Cho, T. Mei, H. Yoshioka, H.  
30 Tian, N. Nishimura, X. Fan, L. J. Guo and Y. Oki, *Opt. Express*, 2018, **26**, 233–241.
- 31 33 C. L. Linslal, S. Sebastian, S. Mathew, P. Radhakrishnan, V. P. N. Nampoori, C. P.  
32 Girijavallabhan and M. Kailasnath, *Appl. Phys. Lett.*, 2015, **106**, 131101.
- 33 34 V. R. Anand, S. Mathew, B. Samuel, P. Radhakrishnan and M. Kailasnath, *Opt. Lett.*,  
34 2017, **42**, 2926–2929.
- 35 35 S. Yang, T. Y. K. Eugene, Y. Wang, X. Zhao, H. V. Demir and H. Sun, *Opt. Express*,  
36 2017, **25**, 2618–2626.
- 37 36 N. Bhardwaj and S. C. Kundu, *Biotechnol. Adv.*, 2010, **28**, 325–347.
- 38 37 A. J. Das, C. Lafargue, M. Lebental, J. Zyss and K. S. Narayan, *Appl. Phys. Lett.*, 2011,  
39 **99**, 263303.
- 40 38 S. Krämmer, C. Vannahme, C. L. C. Smith, T. Grossmann, M. Jenne, S. Schierle, L.  
41 Jørgensen, I. S. Chronakis, A. Kristensen and H. Kalt, *Adv. Mater.*, 2014, **26**, 8096–8100.
- 42 39 A. Camposeo, F. Di Benedetto, R. Stabile, A. A. R. Neves, R. Cingolani and D. Pisignano,  
43 *Small*, 2009, **5**, 562–566.
- 44 40 S. Ubaid, F. Liao, S. Linghu, J. Yu and F. Gu, *Opt. Lett.*, 2018, **43**, 3128–3131.
- 45 41 S. Krämmer, F. Laye, F. Friedrich, C. Vannahme, C. L. C. Smith, A. C. Mendes, I. S.  
46 Chronakis, J. Lahann, A. Kristensen and H. Kalt, *Adv. Opt. Mater.*, 2017, **5**, 1700248.
- 47 42 D. Sun, C. Chang, S. Li and L. Lin, *Nano Lett.*, 2006, **6**, 839–842.
- 48 43 D. Di Camillo, V. Fasano, F. Ruggieri, S. Santucci, L. Lozzi, A. Camposeo and D.

- 1 Pisignano, *Nanoscale*, 2013, **5**, 11637–11642.
- 2 44 G. S. Bisht, G. Canton, A. Mirsepassi, L. Kulinsky, S. Oh, D. Dunn-Rankin and M. J.
- 3 Madou, *Nano Lett.*, 2011, **11**, 1831–1837.
- 4 45 F. Yan, H. Chen, L. Zheng, W. Chen, Y. Liu and Q. Hu, *Adv. J. Food Sci. Technol.*, 2013,
- 5 **5**, 1073–1078.
- 6 46 P. Gaio, F. Cavalieri, E. Chiessi, C. Soagnoli and M. K. Cowman, *J. Electrochem. Soc.*,
- 7 2019, **166**, 687–691.
- 8 47 B. Suo, X. Su, J. Wu, D. Chen, A. Wang and Z. Guo, *Mater. Chem. Phys.*, 2010, **119**, 237–
- 9 242.
- 10 48 K. J. Kim, S. B. Lee and N. W. Han, *Korean J. Chem. Eng.*, 1994, **11**, 41–47.
- 11 49 A. K. Sonker, K. Rathore, R. K. Nagarale and V. Verma, *J. Polym. Environ.*, 2018, **26**,
- 12 1782–1794.
- 13 50 R. P. Shaikh, P. Kumar, Y. E. Choonara, L. C. Du Toit, V. Pillay and L. C. Toit,
- 14 *Biofabrication*, 2012, **4**, 025002.
- 15 51 A. G. Destaye, C. K. Lin and C. K. Lee, *ACS Appl. Mater. Interfaces*, 2013, **5**, 4745–4752.
- 16 52 C. C. Lam, P. T. Leung and K. Young, *J. Opt. Soc. Am. B*, 1992, **9**, 1585–1592.
- 17 53 T. A. Scott, *J. Phys. Chem.*, 1946, **50**, 406–412.
- 18 54 J. H. Wendorff, S. Agarwal and A. Greiner, in *Electrospinning :Materials, Processing, and*
- 19 *Applications*, 2012, pp. 69–104.
- 20 55 J. Pu, X. Yan, Y. Jiang, C. Chang and L. Lin, *Sensors Actuators, A Phys.*, 2010, **164**, 131–
- 21 136.
- 22 56 Y. Huang, Y. Duan, Y. Ding, N. Bu, Y. Pan, N. Lu and Z. Yin, *Sci. Rep.*, 2014, **4**, 5949.
- 23 57 N. Bu, Y. Huang, X. Wang and Z. Yin, *Mater. Manuf. Process.*, 2012, **27**, 1318–1323.
- 24 58 T. Siegle, J. Kellerer, M. Bonenberger, S. Krämmer, C. Klusmann, M. Müller and H. Kalt,
- 25 *Opt. Express*, 2017, **26**, 3579–3593.
- 26 59 M. Sumetsky, *Opt. Lett.*, 2011, **36**, 145–147.
- 27 60 M. Sumetsky, *Int. Conf. Transparent Opt. Networks*, 2011, Tu.B4.3.
- 28 61 F. Luan, E. Magi, T. Gong, I. Kabakova and B. J. Eggleton, *Opt. Lett.*, 2011, **36**, 4761–
- 29 4763.
- 30 62 F. Xie, N. Yao, W. Fang, H. Wang, F. Gu and S. Zhuang, *Photonics Res.*, 2017, **5**, B29–
- 31 B33.
- 32 63 C. Strelow, H. Rehberg, C. M. Schultz, H. Welsch, C. Heyn, D. Heitmann and T. Kipp,
- 33 *Phys. Rev. Lett.*, 2008, **101**, 127403.
- 34 64 T. A. Birks, J. C. Knight and T. E. Dimmick, *IEEE Photonics Technol. Lett.*, 2000, **12**,
- 35 182–183.
- 36 65 J. Wang, T. Zhan, G. Huang, X. Cui, X. Hu and Y. Mei, *Opt. Express*, 2012, **20**, 18555–
- 37 18567.
- 38 66 M. L. Gorodetsky, A. A. Savchenkov and V. S. Ilchenko, *Proc. SPIE - Int. Soc. Opt. Eng.*,
- 39 1996, **2799**, 389–391.
- 40 67 M. Borselli, T. J. Johnson and O. Painter, *Opt. Express*, 2005, **13**, 1515–1530.
- 41 68 M. Kuwata-gonokami and K. Takeda, *Opt. Mater. (Amst).*, 1998, **9**, 12–17.
- 42 69 X. Chen, K. Xie, T. Hu, X. Zhang, Y. Yang, J. Ma, J. Zhang, X. Cheng and Z. Hu, *J. Phys.*
- 43 *D. Appl. Phys.*, 2019, **52**, 475104.
- 44 70 M. Anthamatten, S. a Letts and R. C. Cook, *Langmuir*, 2004, **20**, 6288–96.
- 45 71 V. R. Anand, S. Mathew, C. L. Linslal, P. Radhakrishnan and M. Kailasnath, *J. Lumin.*,
- 46 2019, **209**, 69–73.
- 47 72 M. R. Foreman and F. Vollmer, *Phys. Rev. Lett.*, 2015, **114**, 118001.
- 48 73 J. Zhang, J. Zhong, Y. F. Fang, J. Wang, G. S. Huang, X. G. Cui and Y. F. Mei,

- 1           *Nanoscale*, 2014, **6**, 13646–13650.  
2   74   K. Scholten, X. Fan and E. T. Zellers, *Lab Chip*, 2014, **14**, 3873–3880.  
3   75   M. Charlebois, A. Paquet, L. S. Verret, K. Boissinot, M. Boissinot, M. G. Bergeron and C.  
4   N. Allen, *Nanoscale Res. Lett.*, 2010, **5**, 524–532.  
5   76   A. Weller, F. C. Liu, R. Dahint and M. Himmelhaus, *Appl. Phys. B Lasers Opt.*, 2008, **90**,  
6   561–567.  
7   77   M. Himmelhaus, S. Krishnamoorthy and A. Francois, *Sensors*, 2010, **10**, 6257–6274.  
8   78   S. Kudo, E. Otsuka and A. Suzuki, *J. Polym. Sci. Part B Polym. Phys.*, 2010, **48**, 1978–  
9   1986.  
10  79   K. Kamemaru, S. Usui, Y. Hirashima and A. Suzuki, *Gels*, 2018, **4**, 45.  
11  80   K. J. Kim, S. B. Lee and N. W. Han, *Polym. J.*, 1993, **25**, 1295–1302.  
12

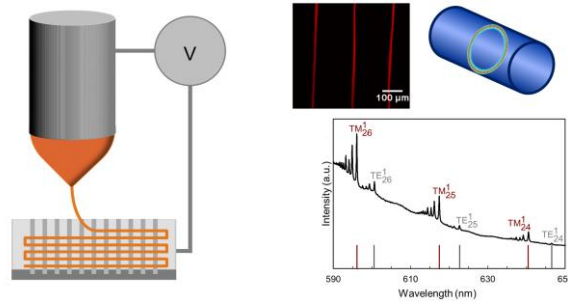
## 13   **7. Footnotes**

14   †Electronic Supporting Information available

15   ‡These authors contributed equally.

16

## Table of Contents Entry



Near-field electrospun polymer microfibers were utilized to support whispering gallery mode resonances. The fibers were utilized for water-ethanol sensing.